This is a public version of the accepted manuscript published in Applied Surface Science https://doi.org/10.1016/j.apsusc.2013.01.061

© 2013. This manuscript version is made available under the CC-BY-NC-ND 4.0 license: https://creativecommons.org/licenses/by-nc-nd/4.0/

Analysis of wavelength influence on a-Si crystallization processes with nanosecond laser sources

O. García [a], J.J. García-Ballesteros [a], David Munoz-Martin [a], S. Núñez-Sánchez [a], M. Morales [a], J. Carabe [b], I. Torres [b], J.J. Gandía [b], C. Molpeceres [a]

[a]Centro Láser UPM, Universidad Politécnica de Madrid, Campus Sur UPM, Edificio La Arboleda Ctra. de Valencia, km. 7,300, 28031 Madrid, Spain

[b]CIEMAT. Av. Complutense 40, 28040 Madrid, Spain

Abstract

In this work we present a detailed study of the wavelength influence in pulsed laser annealing of amorphous silicon thin films, comparing the results for material modification at different fluence regimes in the three fundamental harmonics of standard DPSS (diode pumped solid state) nanosecond laser sources, UV (355 nm), visible (532 nm) and IR (1064 nm).

The crystalline fraction (% crystalline silicon) profiles resulted from irradiation of amorphous silicon thin film samples are characterized with MicroRaman techniques. A finite element numerical model (FEM) is developed in COMSOL to simulate the process. The crystalline fraction results and the local temperature evolution in the irradiated area are presented and analyzed in order to establish relevant correlation between theoretical and experimental results.

For UV (355 nm) and visible (532 nm) wavelengths, the results of the numerical model are presented together with the experimental results, proving that the process can be easily predicted with an essentially physical model based on heat transport at different wavelengths and fluence regimes. The numerical model helps to establish the optimal operation fluence regime for the annealing process.

Keywords

Laser crystallization, Amorphous silicon, COMSOL Multiphysics, Annealing

1 Introduction

Pulsed laser crystallization has been widely applied to formation of polycrystalline silicon films and has been introduced to fabrication process of polycrystalline silicon thin film transistors (poly-Si TFTs) and solar cell applications [1], [2], [3]. Crystallization and grain growth technique of thin film silicon are among the most promising methods for improving efficiency and lowering cost of solar cells.

A major advantage of laser crystallization and annealing over conventional heating methods is its ability to limit rapid heating and cooling to thin surface layers. This is mainly controlled by the pulse duration time and the absorption depth of the laser light used in the material [4].

Laser energy is used to heat the amorphous silicon thin film, melting it and changing the microstructure to polycrystalline silicon (poly-Si) as it cools. Phase change from a-Si to poly-Si depends on the absorbed energy from the incident laser-pulse. Pulsed excimer lasers such as XeCl and KrF have been widely used for annealing of a-Si films [5], [6], [7], [8], [9] due mainly to the strong absorption of UV light in Silicon. However, regarding some limitations of these lasers, numerical and experimental analysis with other wavelengths, like CW diode lasers (808 nm) and pulsed Nd:YAG lasers (532 nm, 355 nm and 1064 nm) have been recently studied [10], [11], [12], [13].

Regarding the proved advantages of DPSS laser sources in production plants, the authors think that experimental and numerical comparative study on local crystallization using the three fundamental harmonics of these laser sources, UV (355 nm), visible (532 nm) and IR (1064 nm), could give useful information for the process implementation in solar cell industry.

In the present work, we report experimental analysis of a-Si local crystallization by a single laser pulse irradiation in these three wavelengths, using nanosecond time regime. Numerical simulation is used to study the energy absorption, phase change and temperature evolution regarding the nanosecond laser pulse interaction on a-Si. The samples are irradiated with different energy regimes in order to evaluate the effect of the laser fluence on the a-Si crystallization. These experimental results are compared with the data obtained from the numerical simulation. We present a different approach for the analysis of the data, explaining some new correlation between numerical and experimental results which can be used to establish the operation range of the process. And as result of this, it is proposed the use of a simple heat transfer model to predict the operation range for DPSS laser sources in the annealing process.

2 Theory

The incident energy of the laser pulse is partially absorbed rising the temperature of the silicon layer. The absorbed light simultaneously excites the electronic states of silicon. The energy of the excited states is relaxed to lattice vibration states within the time on the order of 10^{-12} s. In the case of ns-order pulsed laser irradiation, lattice heat is, therefore, the most important interaction [7]. The heat energy generated at the surface region caused by light absorption diffuses into interior regions of the thin film. When the material is melted and cools down then solidifies to poly-Si phase.

The heating process in the a-Si thin film is governed by the general heat transfer equation:

$$\rho(T)C_p(T)dT/dt=\nabla[k(T)\nabla T]+S \quad (1)$$

where T is the temperature, ρ is the material density, C_p the specific heat and k the thermal conductivity, when a heat source S is considered.

The specific heat, density and thermal conductivity of the material ($C_p(T)$, $k(T)$) are assumed temperature dependent. The source term (S) in Eq. (1) refers to the incident laser beam in the model, which is assumed to be

Gaussian both for the irradiance distribution and the time evolution. The distribution in depth follows the Beer–Lambert law. So, the whole source term $S(r, z, t)$ can be described by the following equation:

(2) $S(r,z,t)=P_i(r,t)[(1-R(T))\alpha(T)\exp(-\alpha(T)|z|)]$

where $\alpha(T)$ is the material absorption coefficient, $R(T)$ the surface reflectivity and P_i the incident laser power (W/m^2) given by the product of the corresponding exponential r and t dependent functions, as follows:

(3) $P_i=Pp\cdot(2/\pi rw^2)\cdot\exp[-2(r/r_w)^2]\exp[-((t-t_0)/(\tau/2))^2]$

where P_p is the peak power, r_w is the beam radius, that is, the half-width at $1/e^2$ of the laser intensity along the radial direction, t_0 the time shift and τ is the time-width of the laser pulse.
The Gaussian fluence profile is given by:

(4) $F(r)=F_p\exp[-2(r/r_w)^2]$

where F_p is the peak fluence, that is, the value of the function F in the center of the laser pulse.
The 2D non-linear heat transfer equation is difficult to solve by analytical approach, so finite element method (FEM) was used to solve it numerically by means of COMSOL multiphysics [14].

2.1 COMSOL multiphysics implementation

According to the mathematical model described before, a heat transfer time-dependent study is applied using *Heat Transfer in Solids* equations with a 2D-axisymmetric model.
Regarding the symmetry and the boundary conditions of the problem, the model is restricted to two dimensions, r and z in cylindrical coordinates system, where r is the distance to the center of the laser pulse and z the depth dimension in the material. The model sample consists of one 2 μm-thick a-Si layer on c-Si substrate. Due to the thickness of the a-Si layer and the maximum laser fluence involved, the substrate is virtually not affected during the process. Therefore the conclusion remains valid when using glass instead of c-Si for the substrate.
The specific heat of a-Si, $C_p(T)$, is replaced by $(C_p(T) + \delta L_m)$ in the heat transfer equation, where L_m is the latent heat of melting and δ is a Gaussian function given in Table 1. The additional term δL_m takes into account the phase change effect within the temperature range of this study [11]. Analogous treatment is made in case of liquid–vapor phase change at the corresponding temperature T_v.

ACCEPTED MANUSCRIPT

Table 1. Thermal properties and parameters used in numerical modeling.

Parameters	Symbol	Value/function		
		532nm	355nm	1064nm
Pulse time-width (ns)	τ	15	17	15
Beam radius (μm)	r_w	20	15	15
Absorption coefficient (solid) (m^{-1})	α_s	1.25e7	1e8	1e6
Reflectivity a-Si (solid)	R_s	0.4	0.54	0.37
Reflectivity a-Si (liquid)	R_l	0.73		
Absorption coefficient (liquid) (m^{-1})	α_l	1e8		
Specific heat ($Jkg^{-1}K^{-1}$)	$C_p(T)$	(952+171×T/685)		
Phase change function	δ	$\frac{1}{\sqrt{\pi}\Delta T}\exp\left(\frac{-(T-T_m)^2}{\Delta T^2}\right)$		
Thermal conductivity (W/(m×K))	$k(T)$	(1.3e−9)×(T−900)^3+(1.3e−7)×(T−900)^2+(1e−4)×(T−900)+1		
Time shift (ns)	t_0	20		
Latent heat (melting) (J/g)	L_m	1320		
Latent heat (vaporization) (J/g)	L_v	13.6e3		
Melting temperature (K)	T_m	1420		
Boiling temperature (K)	T_v	2628		

The boundary conditions applied include initial room temperature, thermal insulation for right, left and bottom boundaries, and finally, surface-to-ambient radiation and convective cooling at the top surface. Absorption coefficient $\alpha(T)$ and surface reflectivity R(T) are taken regarding the wavelength of each laser source. Thermal properties and relevant parameters used for the simulation are listed in Table 1 [10], [15], [16].

The meshing of the model accounts for the laser pulse irradiation area. Therefore a finer meshing is used in the area closest to the center (r = 0) and a coarser meshing is used for the substrate.

The simulation time is 0.5 μs with a maximum time-step of 1 ns. PARDISO direct solver algorithm is used to solve the linear system [17]. The numerical simulation gives the temperature evolution in the sample. The material is heated by a single laser pulse resulting in a fast increase of the a-Si surface temperature. When T_m (1420 K) temperature is reached, the surface begins to melt. Then, the temperature of the melting layer will remain constant until the energy needed for phase change is absorbed. The crystallization of a-Si can take

place not only via melting, but also via solid phase crystallization (SPC), nevertheless, the SPC mechanism is not considered in our numerical model.
Depending on the laser fluence, the vaporization temperature T_v can be reached at the center of the irradiated area. In these cases ablation effects are expected and the annealing process becomes ineffective. As discussed later, the numerical model help to establish the fluence range needed to assure the melting and crystallization without damage or ablation of the silicon surface.

3 Experimental procedure

Two different PECVD systems were used for depositing a-Si:H thin films simultaneously onto glass substrates and onto crystalline silicon wafers from the decomposition of silane (SiH4). The thickness (2 μm) was selected in order to obtain the same amorphous degree in the a-Si deposited on glass and on c-Si and in order to inhibit the pulsed laser induced epitaxial (PLIE) process. Laser irradiation was performed using different fluence regimes in the three fundamental harmonics of standard DPSS laser sources, UV (355 nm), visible (532 nm) and IR (1064 nm), with Gaussian irradiation profile.
The laser sources used in this study were three solid state DPSS laser systems: Nd:YAG Spectra Physics Navigator (30 ns pulse width at 10 kHz repetition rate) for IR (1064 nm) irradiation, Nd:YVO4 Spectra Physics Explorer and Hippo systems (15 ns, and 12 ns pulse width at 50 kHz repetition rate) with fundamental frequency in IR (1064 nm), doubled and tripled to green (532 nm) and UV (355 nm) respectively.
In order to control the number of pulses, lines of irradiated spots were carried out using a scanner. No overlapping of pulses was produced so as to study the crystallization by a single pulse. The morphology of the irradiated area was characterized by confocal laser scanning microscopy (Leica DCM3D).
The structural properties of the irradiated surface were studied by micro-Raman spectroscopy (Renishaw, in Via Raman microscope). The measurements were performed in the range from 200 cm^{-1} to 850 cm^{-1} with a 100X optical microscope objective, scanning the irradiation area with an incident measurement spot of 1 μm diameter. The excitation optical source consisted of an Ar+ laser tuned at the wavelength of 514 nm.
Non irradiated samples show the usual Raman spectrum from the amorphous silicon with a broad band centered at 480 cm^{-1} corresponding to the TO phonon mode [18]. However, the irradiated areas show Raman spectra with two main contributions: one from the amorphous silicon with a broad band localized at 480 cm^{-1} and a second one from the nanocrystalline silicon formed during the laser annealing process with a sharp band centered at 514 cm^{-1}. Due to the large thickness of the a-Si thin films, no residual contribution from the crystalline silicon substrate was observed.
In order to analyze the crystalline fraction (Φ_C) of the irradiated area, the Raman spectra were fitted by three Gaussian line profiles. The center of Gaussian profile contribution of amorphous silicon is set at 480 cm^{-1}. The other two peaks are related to the contribution of the nanocrystalline silicon (Gaussian peak centered on 514 cm^{-1}) and surface modes or silicon defects [19], [20].

4 Results and discussion

The laser fluence is widely identified as a key variable in the crystallization process [4]. The so-called critical fluence (F_c) is used by some authors to identify different crystal-growth regimes [21]. In our study, the fluence regime is used to classify both the numerical (temperature field evolution) and experimental (crystalline fraction) results.
According to the study, the irradiation with IR (1064 nm) wavelength gives qualitative results different to the rest (UV-355 nm and VIS-532 nm). Fig. 1 shows a confocal microscopy image of a single IR pulse laser spot (fluence 1.5 J/cm^2). The outline of the spot and the spattered surrounding area suggest the boiling and ejection of the material. Due to the low absorption coefficient of a-Si at this wavelength, the c-Si substrate behaves as a heat source after the absorption, heating the a-Si layer from the bottom and eventually producing boiling and

material ejection. Although some authors have observed crystallization using 1064 nm [12], in our experiments material ejection takes place mainly due to the longer laser pulse and the higher fluence used with our laser. According to our results, thermal effects associated with pulsed 1064 nm nanosecond laser are a major drawback for laser annealing in the fluence range investigated.

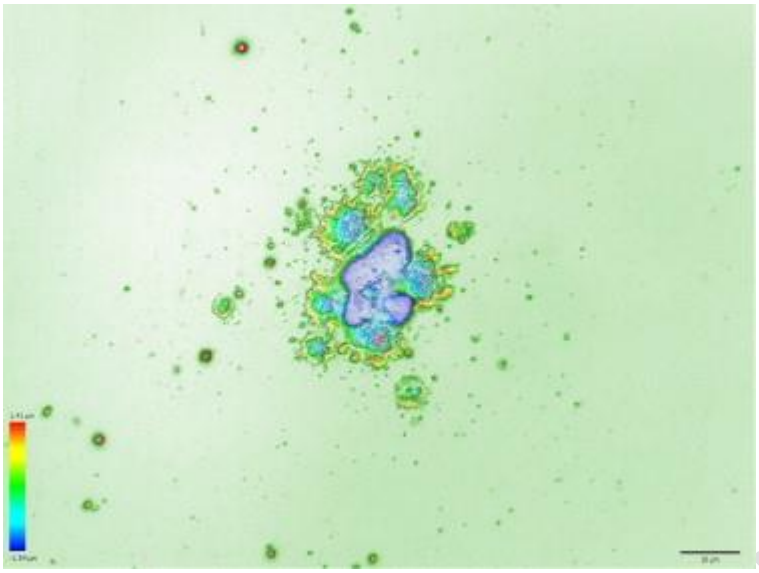

Fig. 1. Confocal microscopy image of a single IR (1064 nm) pulse laser spot (fluence 1.5 J/cm2). The scale reference shown down-right is 10 μm.

As regards to the other wavelengths (UV-355 nm and VIS-532 nm), Fig. 2 shows the comparison between the local fluence profile and the experimental crystalline fraction of two laser spots irradiated with 532 nm laser and two different fluences. It is shown, from top to down, as a function of radius, two Gaussian fluence profiles (2a and 2d) calculated according to Eq. (4) (peak fluence of 240 and 478 mJ/cm^2 respectively), the experimental microscopy images of the irradiated areas (2b and 2e), showing concentric circles which correspond to damaged areas or different crystallization levels, and finally the corresponding crystalline fraction (Φ_C) profile (2c and 2f) obtained by Raman spectroscopy. The crystalline fraction (Φ_C) value of 1 corresponds to 100% polycrystalline silicon. These results shown in Fig. 2 for 532 nm are analogous to those obtained for 355 nm.

ACCEPTED MANUSCRIPT

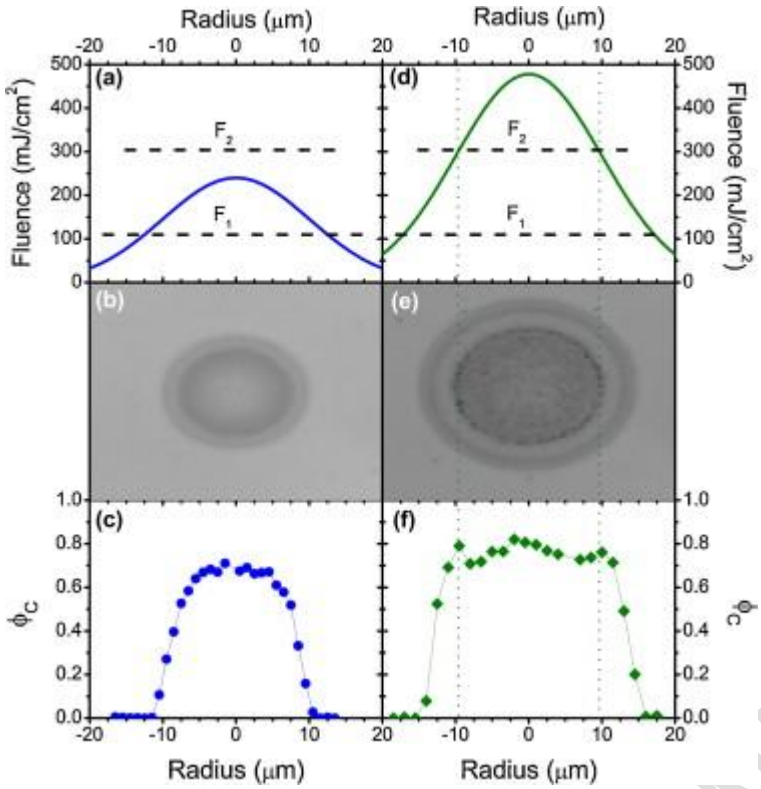

Fig. 2. (a) and (d) Gaussian fluence profile (local fluence as a function of radius) of a green (532 nm) laser pulse. The peak fluence values are 240 mJ/cm^2 (a) and 478 mJ/cm^2 (d). Black dashed lines indicate low (F_1) and high (F_2) fluence thresholds. (b) and (e) Microscope image of the corresponding irradiated areas. The color variation suggests different material crystallization. (c) and (f) Experimental crystalline fraction (Φ_C) profile measured on the surface of the two spots. Again, the peak fluence values are 240 mJ/cm^2 (c) and 478 mJ/cm^2 (f).

In Fig. 2a and d, two fluence thresholds are also shown: the so-called minimum (F_1) and maximum (F_2) fluence threshold. These thresholds are indicated using dash black lines. They have been calculated from the simulation as the fluences leading to a maximum temperature equal to the melting point (1420 K) and the liquid–vapour phase change (2628 K) respectively. At UV-355 nm wavelength the values of F_1 and F_2 are 70 mJ/cm^2 and 374 mJ/cm^2 respectively. At VIS-532 nm wavelength F_1 and F_2 are 110 mJ/cm^2 and 304 mJ/cm^2. According to our study, these values are the limits of the fluence range within which the annealing process should be developed. When the fluence is lower than F_1 the energy of the laser pulse is not enough to melt the silicon surface and therefore Raman results show no crystallization. When the fluence exceeds the F_2 threshold, ablation and damage of the material is expected.

Fig. 2a shows the Gaussian fluence profile of a laser pulse with a peak fluence value of 240 mJ/cm^2. This peak value is in the range limited by F_1 and F_2. According to the profile, the area of the spot located inside a circle of radius ~12 μm is irradiated with fluence larger than F_1, therefore some crystallization is expected here. That is in reasonable agreement with the crystallization profile shown in Fig. 2c. By the other way, this profile shows an increasing crystallization level with a maximum located at the center of the spot. That corresponds to the color variation of different concentric areas, as shown in Fig. 2b, suggesting also different material modification. The maximum level of crystallization achieved in the spot is close to 70% and no crystallization is obtained beyond ~11 μm. No damaged area is observed in the microscope image (2b) and no plateau is shown in the crystallization profile (2c). This is in agreement with the fact that the peak fluence value used in the spot is within the range (F_1, F_2).

Fig. 2d shows the Gaussian profile corresponding to a laser peak fluence of 478 mJ/cm^2. According to this, the area inside a circle of radius ~10 μm is irradiated with fluence larger than F_2. That leads to a damaged area of

radius ~10 μm, which can be seen in Fig. 2e. As mentioned before, in this case the peak fluence exceeds F_2; thus the ablation effect is present and the surface is damaged. The crystalline fraction increases up to reach a plateau (Fig. 2f) corresponding to the damaged area (Fig. 2e). This maximum, constant value of the crystalline fraction (Fig. 2f) is related to the removed material of the surface.

By the other way, according to Fig. 2d, the fluence value is lower than F_1 in the area located outside a circle of radius ~17 μm. That means that the maximum temperature achieved in this area is lower than the melting temperature of amorphous silicon. Thus, no crystallization is expected, which is in agreement with the zero value of Φ_C shown in Fig. 2f.

According to these results, the fluence thresholds F_1 and F_2 predicted by the numerical model are consistent with those experimentally seen. In order to confirm this conclusion with different fluence values in the two wavelengths (355 nm and 532 nm), Fig. 3 shows the maximum temperature from simulation (line) and the crystalline fraction (dotted) measured in the spot, as a function of the fluence, in the two wavelengths (UV-355 nm and VIS-532 nm).

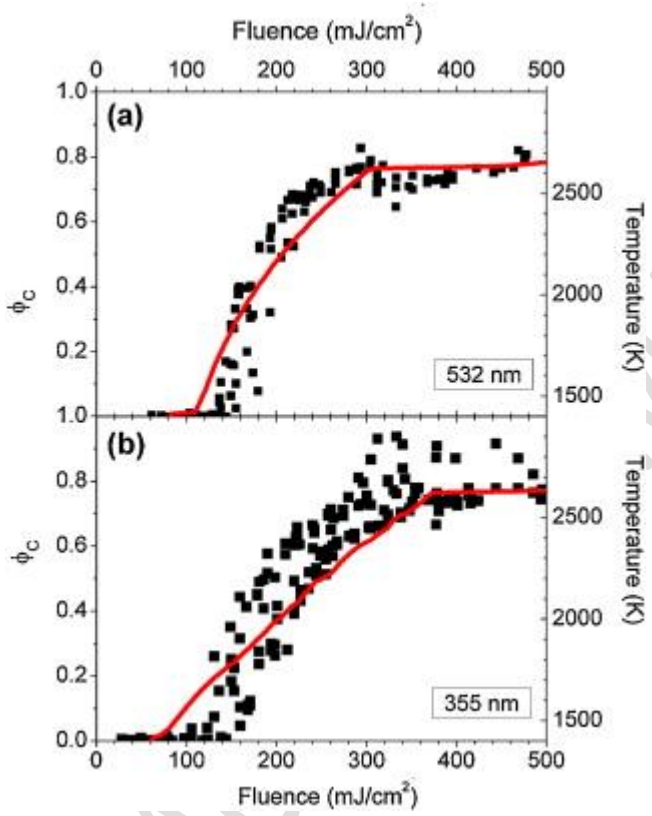

Fig. 3. Maximum surface temperature (line), from simulation, and experimental crystalline fraction ΦC (dotted) versus laser fluence for 532 nm (a) and 355 nm (b). The plateau shown both in the temperature and the crystalline fraction values indicates the high fluence thresholds (F2) in each of the wavelengths.

Again, laser fluence values lower than F_1 lead to maximum temperatures lower than T_m. Thus, no crystallization is achieved. On the other way, when the fluence exceeds F_2, the maximum temperature in the surface reaches the vaporization temperature (T_v), remaining constant when the phase change occurs. In this case ablation occurs and the surface is damaged, leading to a maximum, constant value of the crystalline fraction, as shown in Fig. 3.

When the laser fluence is within the range from F_1 to F_2, the crystalline fraction and the maximum temperature evolution are in good agreement, as Fig. 3 shows. That suggests that the maximum temperature from simulation could be used as an indicator of the expected crystalline fraction in the annealing process.

5 Conclusions

Single pulse laser annealing of a-Si using standard DPSS nanosecond laser sources has been numerically and experimentally investigated.

A transient heat conduction numerical model was implemented in finite element software COMSOL Multiphysics to simulate the process. Experimental values from Raman spectra measurements were used to determine the local crystalline fraction obtained with different laser irradiation fluences and different wavelengths.

The low absorption of a-Si and the thermal effects associated with pulsed 1064 nm nanosecond laser are a major drawback for laser annealing in the fluence range investigated. With regard to the other wavelengths of this study (UV-355 nm and VIS-532 nm), experimental crystalline fraction and numerical results from simulation show reasonable agreement. In these cases the numerical model allows establishing the fluence range within which the annealing process should operate and gives useful information about the expected crystalline fraction depending on the fluence regime and the wavelength used. The fluence thresholds predicted by the numerical model are consistent with those experimentally seen.

On this basis, a process of annealing with multiple overlapped pulses could be designed and optimized. Experimental validation of this issue is subject to further investigation.

Acknowledgements

This work has been supported by the Spanish Ministry of Science and Innovation under projects AMIC ENE2010-21384-C04-02, SIMLASPV ENE2011-23359 and INNDISOL IPT-420000-2010-6 (FEDER funded "Una manera de hacer Europa").

References

[1] A.T. Voutsas, A new era of crystallization: advances in polysilicon crystallization and crystal engineering, Applied Surface Science 208–209 (2003) 250–262.

[2] K. Brendel, N.H. Nickel, P. Lengsfeld, A. Schoepke, I. Sieber, M. Nerding, H.P. Strunk, W. Fuhs, Excimer laser crystallization of amorphous silicon on metal coated glass substrates, Thin Solid Films 427 (2003) 86–90.

[3] A. Luque, S. Hegedus, Handbook of Photovoltaic Science and Engineering, John Wiley & Sons Ltd., England, 2003.

[4] N.H. Nickel, Laser Crystallization of Silicon – Fundamentals to Devices, Semiconductors & Semimetals, vol. 75, Elsevier Academic Press, Netherlands, 2003.

[5] Y.-R. Chen, C.-H. Chang, L.-S. Chao, Modeling experimental analysis in excimer laser crystallization of a-Si films, Journal of Crystal Growth 303 (2007) 199–202.

[6] H. Azuma, A. Takeuchi, T. Ito, H. Fukushima, T. Motohiro, M. Yamaguchi, Pulsed KrF excimer laser annealing of silicon solar cell, Solar Energy Materials & Solar Cells 74 (2002) 289–294.

[7] Sameshima, Laser crystallization for large-area electronics, Applied Physics A: Materials Science & Processing 96 (1) (2009) 137–144.

[8] T. Sameshima, Laser processing for thin film transistor application, Materials Science and Engineering (1997) 186–193.

[9] T. Sameshima, T.H. Watakabe, N. Andoh, S. Higashi, Pulsed laser crystallization of very thin silicon films, Thin Solid Films 487 (2005) 63–66.

[10] Z. Yuan, Q. Lou, J. Zhou, J. Dong, Y. Wei, Z. Wang, H. Zhao, G. Wu, Numerical and experimental analysis on green laser crystallization of amorphous silicon thin films, Optics & Laser Technology 41 (2009) 380–383.

[11] Z. Said-Bacar, Y. Leroy, F. Antoni, A. Slaoui, E. Fogarassy, Modeling of CW laser diode irradiation of amorphous silicon films, Applied Surface Science 257 (2011) 5127–5131.

[12] I.A. Palani, N.J. Vasa, M. Singaperumal, T. Okada, Investigation on laser annealing and subsequent laser-nanotexturing of amorphous silicon (a-Si) films for photovoltaic application, Journal of Laser Micro/Nanoengineering 5 (2) (2010).
[13] B. Bourouga, G. Le Meur, B. Garnier, J.F. Michaud, T. Mohammed-Brahim, Heat transfer during a cw laser crystallization process of a silicon thin film on a glass substrate, in: Excerpt from the Proceedings of the COMSOL Multiphysics User's Conference, Paris, 2005.
[14] COMSOL Multiphysics Reference Manual, version 4.1, COMSOL, AB, 2010.
[15] C.K. Ong, H.S. Tan, E.H. Sin, Calculations of melting threshold energies of crystalline and amorphous materials due to pulsed-laser irradiation, Materials Science and Engineering 79 (1986) 79–85.
[16] G. Poulain, D. Blanc, A. Kaminski, B. Semmache, M. Lemiti, Modeling of laser processing for advanced silicon solar cells, in: Excerpt from the Proceedings of the COMSOL Conference, Paris, 2010.
[17] http://www.pardiso-project.org
[18] C. Smit, R.A.C.M.M. van Swaaij, H. Donker, A.M.H.N. Petit, W.M.M. Kessels, M.C.M. van de Sanden, Determining the material structure of microcrystalline silicon from Raman spectra, Journal of Applied Physics 94 (5) (2003) 3582–3588.
[19] L. Houben, M. Luysberg, P. Hapke, R. Carius, F. Finger, H. Wagner, Structural properties of microcrystalline silicon in the transition from highly crystalline to amorphous growth, Philosophical Magazine a-Physics of Condensed Matter Structure Defects and Mechanical Properties 77 (6) (1998) 1447–1460.
[20] Z. Iqbal, S. Veprek, A.P. Webb, P. Capezzuto, Raman-scattering from small particle-size polycrystalline silicon, Solid State Communications 37 (12) (1981) 993–996.
[21] M. Hatano, S. Moon, M. Lee, C.P. Grigoropoulos, Excimer laser-induced temperature field in melting and resolidification of silicon thin films, Journal of Applied Physics 87 (1) (2000) 36–43

ACCEPTED MANUSCRIPT